Chemistry & Biology, Vol. 12, 339–348, March, 2005, ©2005 Elsevier Ltd All rights reserved. DOI 10.1016/j.chembiol.2005.01.004

Use of the Tubulin Bound Paclitaxel Conformation for Structure-Based Rational Drug Design

Raphaël Geney,[1] Liang Sun,[1] Paula Pera,[2] Ralph J. Bernacki,[2] Shujun Xia,[3] Susan B. Horwitz,[3] Carlos L. Simmerling,[1] and Iwao Ojima[1,*]
[1]Department of Chemistry
State University of New York at Stony Brook
Stony Brook, New York, 11794
[2]Department of Experimental Therapeutics
Roswell Park Cancer Institute
Elm and Carton Streets
Buffalo, New York 14263
[3]Department of Molecular Pharmacology
Albert Einstein College of Medicine
Bronx, New York 10461

Summary

A new computational docking protocol has been developed and used in combination with conformational information inferred from REDOR-NMR experiments on microtubule bound 2-(*p*-fluorobenzoyl)paclitaxel to delineate a unique tubulin binding structure of paclitaxel. A conformationally constrained macrocyclic taxoid bearing a linker between the C-14 and C-3′N positions has been designed and synthesized to enforce this "REDOR-taxol" conformation. The novel taxoid SB-T-2053 inhibits the growth of MCF-7 and LCC-6 human breast cancer cells (wild-type and drug resistant) on the same order of magnitude as paclitaxel. Moreover, SB-T-2053 induces in vitro tubulin polymerization at least as well as paclitaxel, which directly validates our drug design process. These results open a new avenue for drug design of next generation taxoids and other microtubule-stabilizing agents based on the refined structural information of drug-tubulin complexes, in accordance with typical enzyme-inhibitor medicinal chemistry precepts.

Introduction

Taxol (paclitaxel) [1] and Taxotere (docetaxel) [2] (Figure 1) currently serve as two leading chemotherapeutic drugs in the clinic [3–5]. Both drugs bind to the β-tubulin subunit of the α,β-tubulin heterodimer and act through an antimitotic mechanism of action based on stabilization of microtubules (MTBs), thus disrupting the mitosis of cancer cells and eventually leading to apoptosis [6–9].

Over the last two decades, various biological and pharmacological activity data as well as structure-activity relationships have been accumulated on paclitaxel and its congeners (taxoids) [10–12]. The structural biology investigation into the paclitaxel-tubulin interactions has culminated in the determination of the electron crystallographic (EC) structure of the α,β-tubulin heterodimer bound to paclitaxel at 3.7 Å resolution and its subsequent refinement to 3.5 Å resolution [13, 14]. Although representing a seminal achievement, this EC structure lacks the atomic resolution necessary to ascertain the structure of paclitaxel in the β-tubulin binding pocket and the intermolecular interactions responsible for the stabilizing effect of the drug on microtubules.

Solution [15] and solid-phase [16, 17] NMR studies, photolabeling studies [18–20], as well as computational modeling [21–23] have provided additional information regarding the binding structure of paclitaxel. A set of computational protocols described below has been developed in order to unify these highly valuable pieces of information into a more detailed description of the tubulin binding mode of paclitaxel and its analogs.

Synthetic approaches to paclitaxel analogs bearing built-in conformational restrictions have produced the analogs with intrinsically constrained C-13 side chains [24] and the analogs with macrocyclic constraints linking the C-2 and C-3′ positions [21, 25, 26], the C-2 and C-3′N positions [27], as well as the C-4 and C-3′ positions [28]. The syntheses and biological evaluations of these conformationally restricted paclitaxel analogs were performed to identify the bioactive structure of paclitaxel, which may form the basis for the rational design of new generation paclitaxel-like anticancer agents with much simplified structures. However, until very recently [29], none of these restrained analogs displayed in vitro activities equal or superior to paclitaxel. Accordingly, we had a valid concern about the relevance of applying an enzyme-inhibitor complex-type medicinal chemistry approach to the drug-protein interaction involving the highly sophisticated tubulin-microtubule dynamics [8, 9, 30] while we could not obtain a highly active constrained paclitaxel analog. Nevertheless, we did find an analog that exhibited equal or better activity in the tubulin polymerization assay as compared to paclitaxel.

While our computational study was in progress for this highly active analog, Snyder, Kingston, and coworkers reported their results along the same line of research. Their work prompted us to report here our studies on the β-tubulin binding site model for paclitaxel and taxoids on the basis of a new molecular modeling protocol involving the induced-fit of the protein upon drug binding as well as the design, synthesis, and biological activity evaluations of a conformationally restrained paclitaxel analog. The results strongly support the utility of considering the tubulin bound conformation as the bioactive structure of paclitaxel and its use for further rational drug design.

Results and Discussion

Derivation of a Refined Paclitaxel Binding Site Model of β-Tubulin

Conformation of Paclitaxel in β-Tubulin

Solution [15, 31–33] NMR spectroscopy and X-ray crystallography [2, 34] of paclitaxel and its analogs have provided rich information about the various conformations paclitaxel can adopt in the unbound state. This information is only of limited use, since ligands com-

*Correspondence: iojima@notes.cc.sunysb.edu

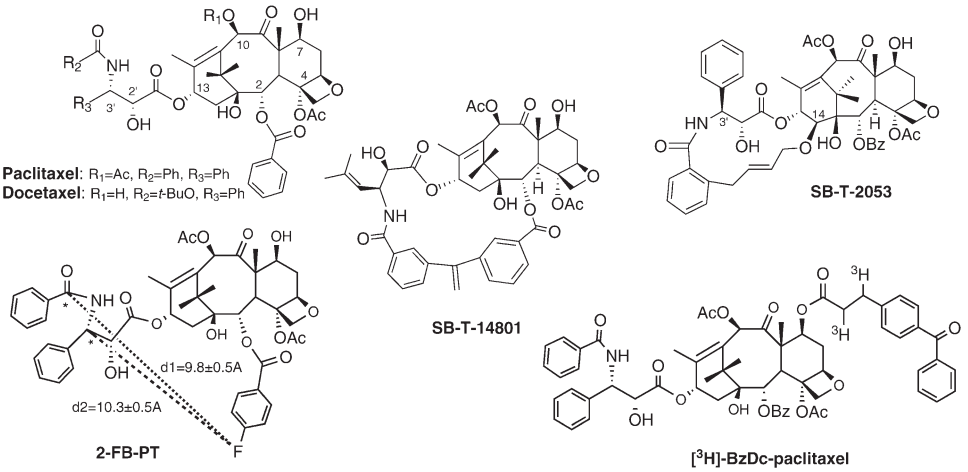

Figure 1. Structures

Structures of paclitaxel, docetaxel, photoaffinity probe [^{3}H]7-BzDc-paclitaxel, and conformationally constrained taxoids SB-T-14801 and SB-T-2053. 2-FB-PT is also shown with intramolecular REDOR-NMR distances indicated.

monly undergo large conformational changes upon binding to their targets [35].

Recently, a fluorinated taxoid, 2-(p-fluorobenzoyl)-paclitaxel (2-FB-PT), was used bound to microtubules in solid state ^{13}C{^{15}N or ^{19}F}-double-REDOR-NMR experiments [17]. After 3 months of data acquisition, Schaefer and his collaborators were able to determine two ^{13}C-^{19}F intramolecular distances for 2-FB-PT in the bound state (d1 and d2 in Figure 1).

Molecular dynamics (MD) simulations were initially conducted on 2-FB-PT in vacuo at increasing temperatures from 300K to 500K (InsightII 2000, Accelrys, CVFF force field). Unfortunately, some side-chain bonds (e.g., C2′-C3′) of the molecule present a high-energy barrier to rotation, impeding adequate sampling. For this reason, we switched to a Monte Carlo (MC) conformational search [36]. The two intramolecular distances determined were then used as constraints in an extensive MC conformational search on 2-FB-PT in vacuo (Macromodel 6.5, Schrödinger, Inc., MM3* forcefield). Conformational diversity in a set of resultant minimized structures was assessed by performing a cluster analysis on the 1371 retained conformations with energies within 50 kJ/mol of the global minimum (Xcluster, Schrödinger, Inc.). Sixteen clusters were formed according to the values of 10 dihedral angles of the C13 and C2 side chains. A representative structure for each cluster is shown in Figure 2. Remarkably, most of these structures have their C3′ benzamido moiety pointing in the same direction as the C2 fluorobenzoate group, as seen for docetaxel in its X-ray structure [2]. Also, to accommodate the REDOR-NMR geometric requirements, the entire C13 side chain has to move away from the C2 fluorobenzoate, unlike in the "hydrophobic collapse" conformation observed for the free drug [31–33].

It should be noted that preliminary unrestrained molecular dynamics simulations on 2-FB-PT (even at elevated temperature, allowing rotation around the C2′-C3′ bond) showed that very few conformations could respect both REDOR distance ranges.

Guided Docking of Taxoids in β-Tubulin

The exact orientation of paclitaxel in β-tubulin has been much debated [17, 20]. Some agreement was nevertheless found between the electron crystallographic density and three photoaffinity labeling experiments [20]. It is worth mentioning that a C7-benzodihydrocinnamoyl (C7-BzDC) derivative of paclitaxel (Figure 1) exclusively labeled the Arg^{282} residue in the M loop of β-tubulin. This specificity prompted us to model the covalent complex thus formed as a single molecule. This way, translational and rotational motions of the ligand are hampered, while the ligand evolves in its most likely position. A two-step procedure was then adopted in order to get a refined binding site model. First, the complex formed by β-tubulin and the bound C7-BzDc paclitaxel in the possible bioactive conformation inferred from the Monte Carlo conformational search was modeled and minimized. The carbonyl carbon of the benzophenone moiety (i.e., as α-hydroxy radical) was connected to the α-carbon of Arg^{282}, since the excited state of the benzophenone moiety would selectively abstract hydrogen from the α position of an amino acid residue because of the capto-dative stabilization of the resulting radical species [37]. The peptide backbone atoms of the protein were kept fixed at all times during the simulation, while side-chain atoms were free to move, allowing the reorganization of side chains upon binding of modified taxoids (partial induced fit). After cleavage of the BzDc linker, a free ligand binding site complex comprising only residues within 10 Å of any ligand or linker atom was minimized again under the same conditions.

The procedure was applied to paclitaxel, starting from all 16 conformations retained from the Monte Carlo conformational search of 2-FB-PT. The REDOR-NMR distances were verified after docking and used as a filter to determine the tubulin bound paclitaxel conformation. However, none of the representative structures could strictly maintain both distances in the allowed REDOR-NMR ranges after docking. Two factors could contribute to this: (1) the availability of large

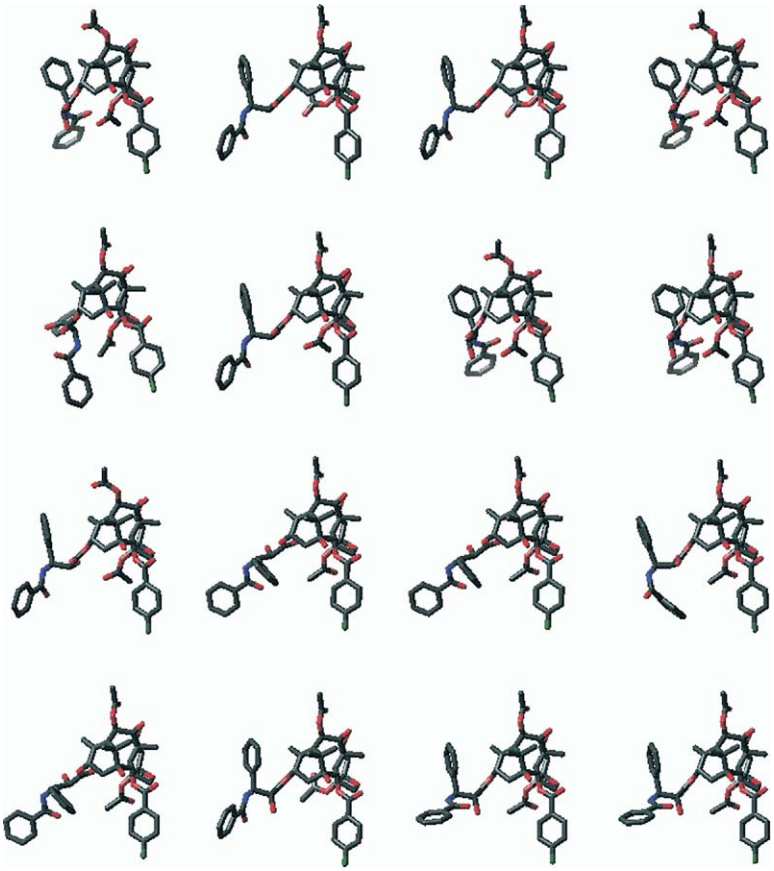

Figure 2. REDOR-NMR Constrained Monte Carlo Conformational Search on 2-FB-PT

Representative structures of the 16 conformational clusters.

empty spaces in the binding site and (2) the fact that the REDOR distances were derived from MTBs, while the EC structure corresponds to the Zn-sheet form of tubulin, which might present some structural differences to the MTB form. The structure deviating the least from the two REDOR-NMR restraints (i.e., d1 = 9.97 Å, d2 = 9.38 Å) was selected as our tubulin bound paclitaxel structure, "REDOR-taxol" (Figure 3).

A significant asset of this guided docking protocol is the total flexibility of the protein side chains during the minimization stages. This allows docking of heavily modified or bulky taxoids under the assumption that their baccatin skeleton remains in the vicinity of paclitaxel in the binding pocket. Figure 4 shows an example of a tubulin bound macrocyclic paclitaxel analog, SB-T-14801, a surprisingly active analog in its series (IC_{50} 60 nM against LCC6) [38]. The protein shows extensive rearrangements induced by the connection of the C2 and C13 taxoid side chains: in particular, the His^{227} side chain has to rotate and face the C2 benzoyl group of the taxoid, confirming that even partial flexibility of the protein allows the binding site to accommodate bulkier analogs.

Analysis of Paclitaxel Binding Site Models

While preliminary results of this work were obtained, producing the "REDOR-taxol" structure [53], Snyder et al. reported a binding site model for paclitaxel by docking 26 experimentally observed unbound paclitaxel conformers into the Zn-sheets EC density map [22]. Although this approach also resulted in an extended bioactive conformation for paclitaxel, "T-taxol," the resolution of the EC map appears insufficient for unequivocal selection of the optimal binding conformation of paclitaxel. It is worth pointing out that T-taxol does not comply with the REDOR-NMR distances, with values of 8.11 Å and 9.32 Å for d1 and d2, respectively (measured on 2-FB-PT in the T-taxol conformation), showing that, in T-taxol, the C-2 and C-3′ side chains are more collapsed than those found with the REDOR-NMR experiment.

The main difference between Snyder's T-taxol and our REDOR-taxol is the conformation of the C13 side chain. In order to fairly compare REDOR-taxol to T-taxol, we docked the T-taxol structure into the β-tubulin binding site using our guided docking protocol (see above). This procedure caused a small but significant realignment of the T-taxol conformation, and an overlay of the resulting pose with REDOR-taxol is shown in Figure 3. The two models locate their C-3′ phenyl rings in nearly identical loci. However, the C2′-hydroxyl group, which usually forms an intramolecular H bond with the C1′-carbonyl oxygen in the free drug, is pointed toward His^{227} in the REDOR-taxol structure, forming a very buried H bond of increased strength. This makes a sharp contrast to the more solvent-exposed H bond between the C2′-hydroxyl and the backbone carbonyl oxygen of Arg^{359} in the T-taxol binding pose.

Additionally, the internal energy of the "free form" of

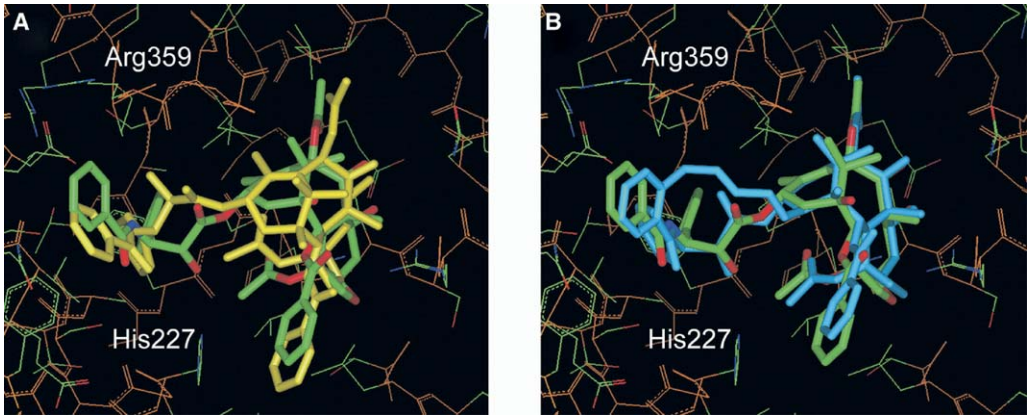

Figure 3. Proposed β-Tubulin Binding Models of Paclitaxel

(A) Overlay of the docked REDOR-taxol (green) and T-taxol (yellow) structures.

(B) Overlay of REDOR-taxol (green) with SB-T-2053 (blue). The overlay is performed by matching the protein backbone, which is kept fixed during docking.

paclitaxel detached from tubulin in vacuo is ~42 kJ/mol lower in the REDOR-taxol conformation than in the T-taxol conformation (CVFF force field, InsightII). This energy difference mostly arises from torsional terms and would suggest that REDOR-taxol requires less stabilization from the protein to make the overall association favorable.

However, due to the low resolution of the tubulin EC density map, direct experimental evidence is lacking to confirm or rule out one of these two conformations as the bioactive form, assuming it is unique.

Design and Synthesis of Conformationally Restrained Macrocyclic Taxoids

Upon visualizing the paclitaxel binding site model of β-tubulin, we noticed unoccupied spaces around the paclitaxel structure. Following a typical enzyme-inhibitor design methodology, we set off to introduce conformational constraints to lower the conformational entropy loss upon binding. These structural modifications should cause minimal disruption to the binding interactions in filling in the empty volumes and possibly add further stabilizing interactions with the protein.

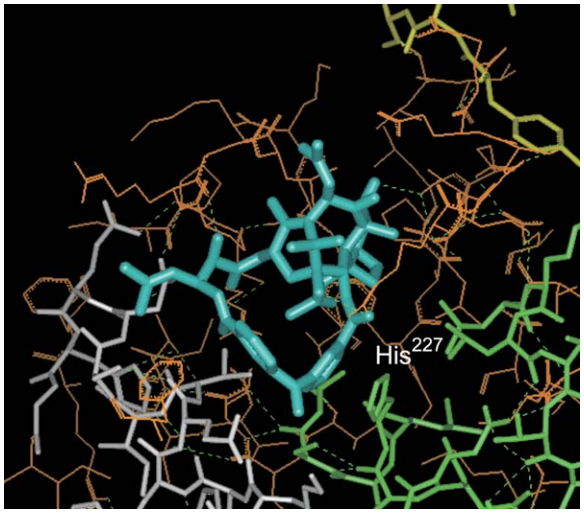

Figure 4. Docked Complex of SB-T-14801

Conformational Restriction to the Binding Conformation

The docked REDOR-taxol structure disclosed a possibility of inserting a hydrophobic linking moiety in the vast hydrophobic cluster formed by the C3′N and C2 benzoyl groups and the imidazol moiety of His[227]. Accordingly, we designed a C14-C3′N-linked taxoid, SB-T-2053 (Figure 1), in which a short (five atoms) linker locks the C3′N side chain in an unequivocal conformation close to REDOR-taxol. Inserting a linker between the C14 and C3′N positions also presents only a small risk of disrupting the original binding of the drug, since the linker moiety lies toward the solvent-exposed surface of the binding site and hence should not generate unfavorable contacts with the protein.

In order to measure the level of conformational restriction imposed, we conducted a Monte Carlo conformational search on SB-T-2053 in a simulated aqueous environment. Performing the same calculation on paclitaxel provided a reference state from which the perturbation can be assessed. Our attention focused on the C-13 side chain dihedral angles since they should be the ones most affected by the introduction of the constraint. Figure 5 shows the dihedral angle distributions for both SB-T-2053 and paclitaxel and compares those to the reference values of REDOR-taxol and T-taxol. The C13-O13 torsion angle remains quite distributed in SB-T-2053, covering the same range as paclitaxel with surprisingly low propensity for the –105° and –150° peaks seen for paclitaxel. The next torsion angle, around O13-C1′, is for the ester linkage and is mostly centered on 0°. However, paclitaxel in solution also adopts the reversed conformation (i.e., 180°) to a lesser extent, contrary to SB-T-2053. The last two dihedral angles, around C1′-C2′ and C2′-C3′, are where the most flexibility is observed in paclitaxel. Indeed, except for

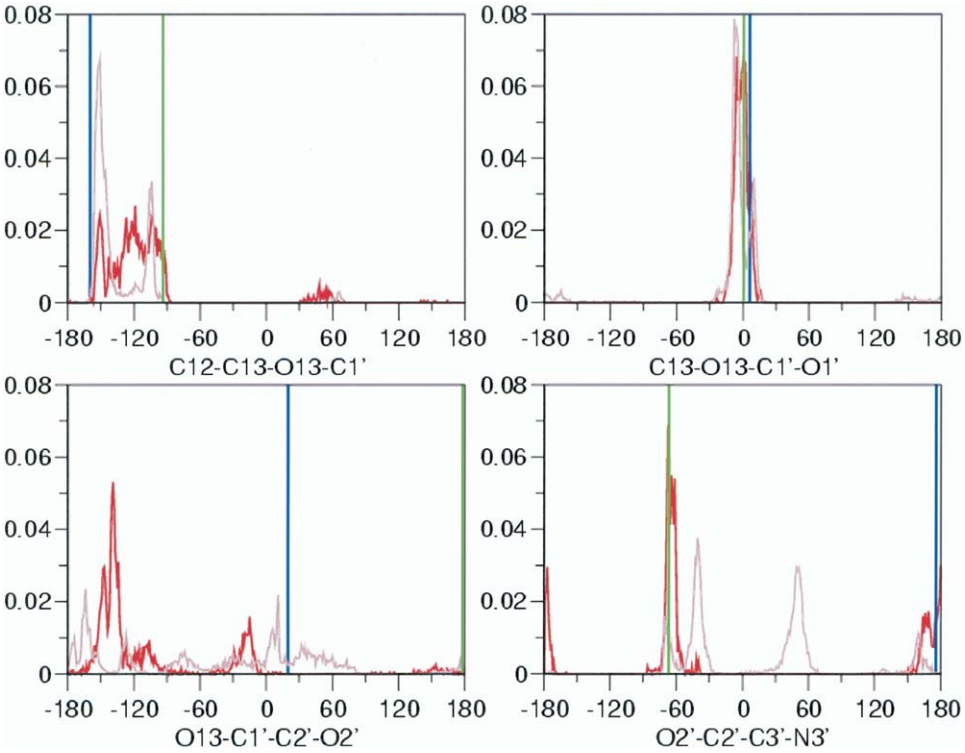

Figure 5. Conformational Diversity in Constrained Taxoid SB-T-2053

Comparison of the C-13 side-chain dihedral angle distributions for paclitaxel (brown) and SB-T-2053 (red) in water. The reference values for REDOR-taxol (blue) and T-taxol (green) are indicated by vertical lines.

the 90° to 150° region, the O13-C1′-C2′-O2′ dihedral angle can adopt every value, with peaks at 10°, –30°, –75°, –120°, and –165°. In sharp contrast, SB-T-2053 does not show any density between 0° and 90°. In the 50 kJ/mol energy range scrutinized, no SB-T-2053 structure was detected that matched REDOR-taxol or T-taxol. However, a peak of the probability density exists near each of the two reference conformations at –15° and –150°. In addition, the T-taxol value should be quite unfavorable since it corresponds to a fully eclipsed conformation.

The O2′-C2′-C3′-N3′ dihedral angle distribution shows the most striking effects of the conformational constraint: while paclitaxel exists in four major conformations, SB-T-2053 is restricted to only two, each of them reproducing the value observed in either REDOR-taxol (176°) or T-taxol (-67°). Therefore, we conclude that the constraint introduced is quite effective in restricting conformational diversity while enriching the solution ensemble in bioactive conformations.

Additionally, very little reorganization of protein side chains is observed after docking of SB-T-2053 as compared to REDOR-taxol (Figure 3), confirming the benign nature of our perturbation on intermolecular interactions.

Synthesis of SB-T-2053

We employed the ring-closing metathesis (RCM) [39] as the key reaction for the synthesis of SB-T-2053 based on our previous successful applications of this protocol in constructing the C2-C3′-linked [21, 25] and C2-C3′N-linked [27] macrocyclic taxoids. The diene precursor for RCM was synthesized through the highly efficient β-lactam-baccatin ring-opening coupling protocol [40–42].

The C-13 side-chain precursor of SB-T-2053, β-lactam **7**, was prepared as shown in Figure 6. β-Lactam **5** [43] was treated with 2-allylbenzoyl chloride **6** [44] to give the desired β-lactam **7** in 91% yield.

In order to construct the C14-C3′N linkage, we introduced an olefin moiety at the C14 position of baccatin. This was realized by allylation of 14β-hydroxy-7-TES-baccatin (**4**) derived from naturally occurring 14β-hydroxy-10-deacetylbaccatin (14β-OH-10-DAB, **1**) [45]. As Figure 6 shows, baccatin **1** was first treated with acetic anhydride in the presence of cerium chloride to afford 10-Ac-14β-OH-10-DAB **2**. Then, selective TES protection of the C7-OH using TESCl and imidazole gave 7-TES-14-OH-baccatin (**3**) in 83% yield over two steps. Finally, in the presence of NaHMDS, **3** was treated with allyl iodide to afford **4** bearing an allyl ether moiety at the C-14 position. The ring-opening coupling of β-lactam **7** with baccatin **4** gave diene **8** in 72% yield. RCM reaction afforded the desired macrocyclic taxoid **9** in 85% yield. Finally, the silyl groups were removed using HF-pyridine to yield SB-T-2053 (E-isomer only).

Biological Evaluation of Conformationally Constrained Taxoid SB-T-2053

The activities of SB-T-2053 and paclitaxel were compared in an in vitro tubulin polymerization assay.

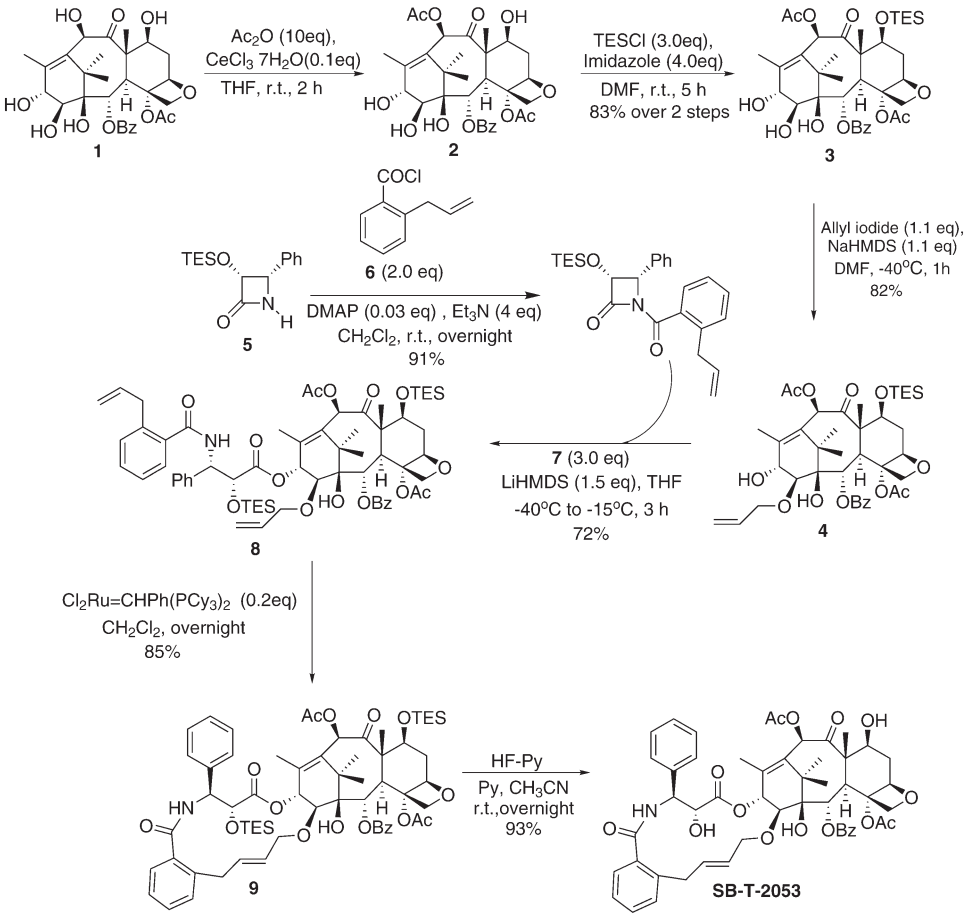

Figure 6. Synthesis of C14-C3′N Linked Taxoid SB-T-2053

Changes in absorbance in this assay indicate the extent of microtubule polymerization. SB-T-2053, like paclitaxel, induces tubulin polymerization in the absence of GTP, which is normally required for microtubule assembly. Furthermore, the microtubules formed in the presence of SB-T-2053 and paclitaxel were both stable against calcium-induced depolymerization (see Figure S1). The calculated critical concentration of protein required to achieve assembly is approximately 0.08 mg tubulin/ml for both drugs (data not shown). As indicated in Figures 7A and 7B, both drugs polymerize tubulin to a similar extent over a range of different ratios of tubulin to drug. Furthermore, a competitive binding assay indicated that both paclitaxel and SB-T-2053 effectively displace [^{3}H]paclitaxel from microtubules (see Figure S2). This result provides further strong supporting evidence that SB-T-2053 binds to the paclitaxel binding site on the microtubule.

The macrocyclic taxoid SB-T-2053 also exhibits strong potency against LCC6-WT and MCF-7 human breast cancer cell lines with IC_{50} values of 15 and 42 nM, respectively (Figure 7C). The former growth inhibition is only 3.3 times less potent than paclitaxel against the same cell line. Considering that SB-T-2053 is comparable to paclitaxel as an inducer of microtubule polymerization, the small differences in IC_{50} values between paclitaxel and SB-T-2053 could be due to cell permeability and solubility factors of two distinct molecules. Also, SB-T-2053 exhibits the same level of potency as paclitaxel against multidrug-resistant human breast cancer cell lines (LCC6-MDR and MCF7-R) overexpressing P-glycoprotein [46, 47].

Significance

A new bioactive structure of paclitaxel, REDOR-taxol, has been identified on the basis of detailed computational analysis of the combined data from REDOR-NMR, electron crystallography, and photoaffinity labeling experiments. Although the REDOR-taxol structure shares similar features with Snyder's T-taxol [22], the REDOR-taxol structure allows a strong H bonding between the C2′ hydroxyl group of paclitaxel and the His^{227} residue, in contrast to T-taxol, which has H bonding between C2′-OH and Arg^{359} in the S9-S10 loop. The REDOR-taxol structure was used to design a conformationally constrained taxoid, wherein the C3′N-pharmacophoric group is restrained directly to the C14 of the baccatin skeleton with little or no impact on other key pharmacophoric groups and causing minimal unfavorable interactions with the target protein. We have successfully synthesized SB-T-

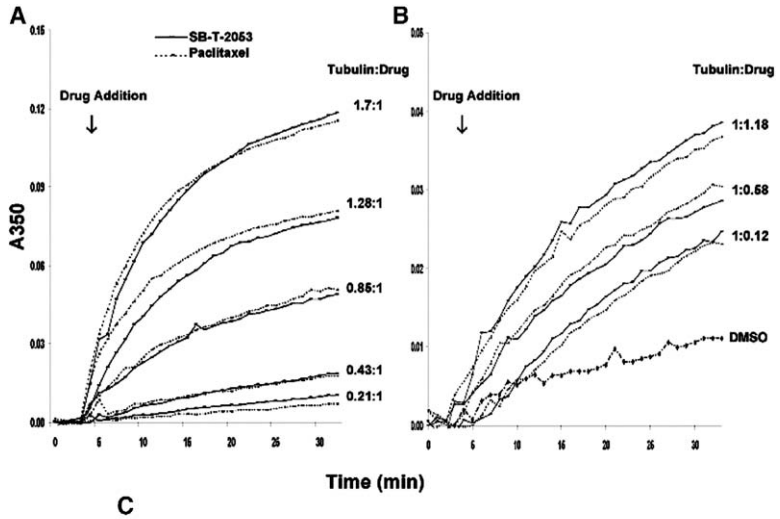

Figure 7. Compared In Vitro Bioactivities of SB-T-2053 and Paclitaxel

(A and B) Tubulin polymerization and microtubule stabilization assay for 5 μM paclitaxel or SB-T-2053 and various concentrations of tubulin (A), 5 mg/ml tubulin and various concentrations of drug (B).

(C) Growth inhibition assay IC_{50} values, nM (concentration of compound inhibiting 50% of the growth of human tumor cell line after 72 hr drug exposure); LCC6-WT, human breast carcinoma; LCC6-MDR, MDR1 transducedline; MCF7-S, human breast carcinoma; MCF7-R, MDR phenotype human breast carcinoma.

C

Taxoid	LCC6-WT[b]	LCC6-MDR[c]	MCF7-S[d]	MCF7-R[e]
Paclitaxel	4.5±0.8	323±23	3.0±0.3	518±71
SB-T-2053	15±1.6	455±38	42±2.3	1066±59

2053, a C14-C3′N-linked macrocyclic taxoid using RCM in the key step. Molecular modeling anticipates decreased conformational flexibility for the C13 side chain of SB-T-2053 while still allowing the adoption of either REDOR-taxol or T-taxol conformation.

The macrocyclic taxoid SB-T-2053 possesses significant potency against human breast cancer cell lines comparable to that of paclitaxel. Moreover, SB-T-2053 induces tubulin polymerization in vitro at least as well as paclitaxel, which directly validates our design process.

This example of successful conformational restriction corroborates the very recent report by Snyder, Kingston, and their collaborators, wherein C4-C3′-phenyl-linked analogs of paclitaxel were shown to be at least as active as paclitaxel against cancer cell lines as well as in tubulin binding and tubulin-polymerization assays [29]. These highly encouraging results obtained by us and others have opened a new avenue for drug design and discovery of new-generation taxoids as well as new microtubule-stabilizing agents based on the refined structural information of drug-protein complexes in accordance with a typical enzyme-inhibitor medicinal chemistry approach.

Experimental Procedures

Computational Methods

2-FB-PT was modeled after the X-ray structure of paclitaxel [34] in Macromodel 6.5 (Schrödinger) by substituting an F atom on the *para* position of the C2 benzoate group. Monte Carlo conformational searching was conducted with energy minimization on the isolated 2-FB-PT molecule in the gas phase (4000 MC steps, minimization for 1000 steps with Polak-Ribiere conjugated gradients) using the MM3* force field, well suited for the conformational analysis of small molecules. All side-chain rotatable bonds were allowed to vary. 1371 structures were found within 50 kJ/mol, which complied with both REDOR NMR distances. These conformers were clustered according to their C13 and C2 side chains' dihedral angles using the Xcluster facility packaged with Macromodel 6.1. Sixteen clusters were obtained at the 1356 clustering level, comprising 124, 250, 76, 236, 1, 129, 243, 220, 69, 1, 1, 1, 2, 1, 1, and 16 members, respectively. A representative structure for each cluster was selected as the structure with minimal root-mean-square distance to the centroid of all cluster members, regardless of its energy relative to the global minimum of the conformational search.

All 16 representative conformations of paclitaxel were then docked into the paclitaxel binding site of β-tubulin following the same procedure: their taxane skeleton (carbon atoms of the A, B, and C rings) was overlaid with those of docetaxel present in the deposited β-tubulin EC structure (Protein Data Bank ID code 1TUB). The BzDc linker was modeled and attached to C7 of paclitaxel in InsightII 2000 (Accelrys Inc.). Finally, the linker was attached to the Cα of Arg^{282} by merging the two fragments, thus creating an elongated C-C bond.

The molecular complex was allowed to minimize for 1000 steps with the conjugate gradients method, CVFF force field, and distance-dependent dielectric. The BzDc linker was then erased, and H atoms were added to reconstitute the free paclitaxel ligand and the protein after a binding domain comprising all residues within 10 Å of the bound 7-BzDc-PTX had been defined. A second minimization was then conducted on the noncovalent complex of paclitaxel with this 10 Å binding domain (same conditions as first minimization). The approach was identical for all the taxoids docked.

Monte Carlo conformational searches on paclitaxel and SB-T-2053 were performed in Macromodel 6.5 using a generalized born with surface area term (GBSA) continuum solvent description of water solvation [48]. Other conditions were identical to the 2-FB-PT MC conformational search, except that no distance restraint was used.

Tubulin Polymerization Assay

Assembly and disassembly of calf brain microtubule protein (MTP) was monitored spectrophotometrically (Beckman Coulter DU 640, Fullerton, CA) by recording changes in turbidity at 350 nm at 37°C [49, 50]. MTP was diluted to 1 mg/ml in MES buffer containing 3 M glycerol. The concentration of tubulin in MTP was 85%, and that was taken into consideration when the ratios of tubulin to drug

were presented in Figures 7A and 7B. Microtubule assembly was done with 5 μM paclitaxel or SB-T-2053 and various concentrations of tubulin or with 5 mg/ml tubulin and various concentations of drug. Calcium chloride (6 mM) was added to the assembly reaction after 90 min to follow the calcium-induced microtubule depolymerization.

Competitive Binding Assay

[^{3}H]paclitaxel (specific activity 19.3Ci/mmol, 15.89 μM in toluene) was dried and dissolved with cold paclitaxel in dimethyl sulfoxide to a final concentration of 500 μM. [^{3}H]paclitaxel, different concentrations of the competing compounds, or dimethyl sulfoxide was added to MTP (2 μM) in MES buffer containing 0.2 mM GTP. After incubation for 2 hr at 37°C, samples were layered onto 5% sucrose in MES buffer with 3 M glycerol and centrifuged in a Ti42.2 rotor in a Beckman L7 ultracentrifuge (Beckman Instruments, Inc., CA) at 100,000 × g for 1 hr at 27°C. After centrifugation, the supernatant was carefully removed. The pellet was washed three times with MES buffer and dissolved in 10 mM sodium phosphate buffer containing 1% SDS. Radioactivity was determined in a liquid scintillation counter (PerkinElmer, IL). Protein concentration was measured by DC Protein Assay (Bio-Rad Laboratories, CA). After correcting for small amounts of nonspecifically sedimented protein, the ratio between [^{3}H]paclitaxel and tubulin dimer was calculated.

In Vitro Growth Inhibition Assay

Tumor-cell growth inhibition was determined according to the method established by Skehan et al. [51]. Human breast carcinoma cells MCF-7, LCC6, and their Pgp-expressing variants, MCF7-R and LCC6-MDR, were plated at a density of 400–2000 cells/well in 96-well plates and allowed to attach overnight. These cell lines were maintained in RPMI-1640 medium (Roswell Park Memorial Institute growth medium) supplemented with 5% fetal bovine serum and 5% Nu serum (Collaborative Biomedical Product, MA). Taxanes were solubilized in DMSO and further diluted with RPMI-1640 medium. Triplicate wells were exposed to various treatments. After 72 hr incubation, 100 μl of ice-cold 50% trichloroacetic acid (TCA) was added to each well, and the samples were incubated for 1 hr at 4°C. Plates were then washed five times with water to remove TCA and serum proteins, and 50 μl of 0.4% sulforhodamine B (SRB) was added to each well. Following a 5 min incubation, plates were rinsed five times with 0.1% acetic acid and air dried. The dye was then solubilized with 10 mM Tris base (pH 10.5) for 5 min on a gyratory shaker. Optical density was measured at 570 nm. The IC_{50} values were then calculated by fitting the concentration-effect curve data with the sigmoid-E_{max} model using nonlinear regression weighted by the reciprocal of the square of the predicted effect [52].

General Synthetic Procedures

Chemicals and reagents were purchased from Sigma-Aldrich or Fisher Scientific and were used without further purification unless otherwise noted. 14β-hydroxy-10-deacetylbaccatin III was a gift from Indena, SpA and used as received. Solvents were reagent grade and freshly distilled under nitrogen before use. ^{1}H and ^{13}C NMR spectra were measured on a Bruker AC-250 NMR spectrometer or Varian 300, 400, 500 NMR spectrometers using tetramethylsilane as the internal standard. Melting points were measured on a Thomas Hoover Capillary melting point apparatus and are uncorrected. Optical rotations were measured on a Perkin-Elmer Model 241 polarimeter. TLC was performed on Merck DC-alufolien with Kieselgel 60F-254, and column chromatography was carried out on silica gel 60 (Merck; 230–400 mesh ASTM). High-resolution mass spectra were obtained from the Mass Spectrometry Laboratory, University of Illinois at Urbana-Champaign, Urbana, IL.

14β-Hydroxybaccatin III (2)

To a solution of 14β-hydroxy-10-deacetylbaccatin III (1) (200 mg, 0.37 mmol) in 13 ml of THF was added $CeCl_3.7H_2O$ (16 mg, 0.037 mmol) and acetic anhydride (0.5 ml, 3.7 mmol). The reaction mixture was then stirred 2 hr at room temperature and quenched with a saturated aqueous $NaHCO_3$ solution (10 ml). The mixture was then extracted with EtOAc (30 ml × 3), washed with brine (15 ml), dried over anhydrous $MgSO_4$, and concentrated in vacuo. The crude product was used directly for the next step without further purification as a white solid (256 mg).

7-Triethylsilyl-14β-Hydroxybaccatin III (3)

To a solution of 14β-hydroxybaccatin III (**2**) (222 mg, 0.37 mmol) and imidazole (98 mg, 1.08 mmol) in DMF (5 ml) was added chlorotriethylsilane (0.18 ml, 1.08 mmol) dropwise via syringe at room temperature. The reaction mixture was then stirred for 5 hr at room temperature, quenched by saturated NH_4Cl, and extracted with EtOAc (30 ml × 3). The mixture was then washed with H_2O (10 ml × 2), brine (10 ml), dried over anhydrous $MgSO_4$, and concentrated. The crude product was purified on a silica gel column using hexanes/EtOAc (2/1 followed by 1/1) as the eluent to give **3** as a white solid (219 mg, 83% over 2 steps). Mp 164°C –166°C. ^{1}H NMR (300 MHz, $CDCl_3$) δ 0.58 (m, 6 H), 0.91 (m, 9 H), 1.02 (s, 3 H), 1.22 (s, 3 H), 1.68 (s, 3 H), 1.86 (m, 1 H) (H6a), 2.14 (s, 3 H), 2.17 (s, 3 H) (OAc), 2.28 (s, 3 H) (OAc), 2.50 (m, 1 H) (H6b), 3.26 (br s, 1 H), 3.61 (s, 1 H), 3.79 (br s, 1 H), 3.80 (d, *J* = 7.2 Hz, 1 H) (H3), 4.01 (d, *J* = 6.3 Hz, 1 H) (H14), 4.16 (d, *J* = 8.3 Hz, 1 H) (H20a), 4.24 (d, *J* = 8.3 Hz, 1 H) (H20b), 4.46 (dd, *J* = 6.5, 10.3 Hz, 1 H) (H7), 4.67 (d, *J* = 5.5 Hz, 1 H), 4.93 (d, *J* = 8.7 Hz, 1 H) (H5), 5.78 (d, *J* = 7.2 Hz, 1 H) (H2), 6.43 (s, 1 H) (H10), 7.41 (t, *J* = 7.5 Hz, 2 H), 7.55 (t, *J* = 7.5 Hz, 1 H), 8.02 (d, *J* = 7.4 Hz, 2 H). ^{13}C NMR (62.9 MHz, $CDCl_3$) δ 5.2, 6.7, 10.0, 14.6, 20.8, 21.8, 22.3, 26.2, 37.1, 42.8, 46.5, 58.6, 72.2, 74.1, 74.3, 75.5, 76.3, 76.7, 80.7, 84.1, 128.6, 129.3, 133.5, 141.3, 165.4, 169.3, 170.3, 202.3. HRMS (FAB/DCM/NaCl) m/z calculated for $C_{37}H_{52}O_{12}SiH^+$: 717.3306, found: 717.3276.

14-Allyl-7-Triethylsilyl-14β-Hydroxybaccatin III (4)

To a solution of **3** (63 mg, 0.09 mmol) in DMF (3 ml) was added NaHMDS (1.0 M in THF, 0.1 ml, 0.1 mmol) at –40°C. The reaction mixture was stirred for 5 min, and then allyl iodide (0.012 ml, 0.1 mmol) was added. The reaction was quenched after 1 hr with a saturated aqueous NH_4Cl solution (20 ml) and extracted with EtOAc (30 ml × 3) and washed with H_2O (10 ml × 2) and brine (10 ml). The organic layer was dried over anhydrous $MgSO_4$, filtered, and the solvent was removed under reduced pressure. The residue was purified on a silica gel column using hexanes/EtOAc (5/1) as the eluent to afford **4** as a white solid (74 mg, 82%). Mp: 133°C–135°C. ^{1}H NMR (300 MHz, $CDCl_3$) δ 0.55 (m, 6 H), 0.90 (m, 9 H), 1.19 (s, 3 H), 1.60 (m, 2 H), 1.66 (s, 3 H), 1.84 (m, 1 H), 2.00 (m, 3 H), 2.12 (s, 3 H), 2.29 (s, 3 H), 2.50 (m, 1 H), 3.22 (d, *J* = 4.2 Hz, 1 H), 3.69 (d, *J* = 5.7 Hz, 1 H), 3.77 (m, 2 H), 4.06 (m, 1 H), 4.18 (m, 1 H), 4.29-4.47 (m, 3 H), 4.69 (bs, 1 H), 4.87–4.98 (m, 3 H), 5.61–5.72 (m, 1 H), 5.83 (d, *J* = 6.9 Hz, 1 H), 7.42 (m, 2 H), 7.55 (m, 1 H), 8.06 (m, 2 H). ^{13}C NMR (62.9 MHz, $CDCl_3$) δ 5.1, 5.4, 6.6, 6.7, 9.7, 10.0, 14.7, 20.8, 21.4, 22.4, 26.2, 37.1, 42.7, 46.4, 58.7, 72.1, 73.0, 74.5, 75.6, 75.7, 76.2, 76.4, 80.9, 81.5, 82.0, 84.0, 117.4, 128.4, 129.7, 129.8, 133.3, 133.6, 133.7, 141.2, 165.6, 169.3, 170.1, 201.9. HRMS (FAB/DCM/NaCl) m/z calculated for $C_{40}H_{56}O_{12}SiH^+$: 757.3619, found: 757.3643.

(*3R,4S*)-1-(2-Allylbenzoyl)-3-Triethylsilyloxy-4-Phenylazetidin-2-One (7)

To a solution of β-lactam **5** (60 mg, 0.216 mmol), triethylamine (0.13 ml, 0.912 mmol), and DMAP (7 mg, 0.06 mmol) in 2.4 ml CH_2Cl_2 was added 2-allylbenzoyl chloride in CH_2Cl_2 (2 ml) dropwise at room temperature. The mixture was stirred overnight at room temperature, and the reaction was quenched with a saturated aqueous NH_4Cl solution (20 ml). The mixture was then extracted with ethyl acetate (30 ml × 3). The combined extracts were dried over anhydrous $MgSO_4$ and concentrated in vacuo. The crude product was purified on a silica gel column using hexanes/EtOAc (25/1) as the eluent to afford **7** as a colorless oil (97 mg, 91% yield): ^{1}H NMR (400 MHz, $CDCl_3$) δ 0.42 (m, 6 H), 0.77 (m, 9 H), 3.48 (dd, *J* = 15.6, 6.0 Hz, 1 H), 3.58 (dd, *J* = 15.6, 6.4 Hz, 1 H, 5.01 (m, 2 H), 5.14 (d, *J* = 6.4 Hz, 1 H), 5.33 (d, *J* = 17.5, 6.4 Hz, 1 H), 5.93 (m, 1 H), 7.30 (m, 7 H), 7.4 (dd, *J* = 8.8, 6.8 Hz, 1 H), 7.57 (d, *J* = 6.8 Hz, 1 H), ^{13}C NMR (100.5 MHz, $CDCl_3$) δ 4.3, 6.2, 37.2, 61.3, 76.7, 115.9, 125.9, 128.0, 128.1, 128.3, 128.8, 130.2, 131.4, 133.1, 133.6, 136.9, 138.9, 165.4, 166.6. HRMS (FAB/DCM/NaCl) m/z calculated for $C_{25}H_{31}NO_3SiH^+$: 422.2151, found: 422.2153.

14β-Alloxy-3′*N*-Debenzoyl-3′*N*-(2-Allylbenzoyl)-7,2′-Triethylsilylpaclitaxel (8)

To a solution of **4** (20 mg, 0.026 mmol) and β-lactam **7** (33 mg, 0.079 mmol) in THF (2.8 ml) was added LiHMDS (0.04 ml, 0.04 mmol) at –40°C. The reaction mixture was warmed up to –20°C over 3 hr and then quenched with a saturated aqueous NH_4Cl solution and extracted with EtOAc. The organic layers were combined and solvent was removed under reduced pressure. The residue was purified by chromatography (eluent Hex/EtOAc, 7/1) to afford **8** as a white solid. (22 mg, 72%). Mp: 99°C –102°C. ^{1}H NMR (500 MHz, $CDCl_3$) δ 0.35–0.47 (m, 6 H), 0.55–0.63 (m, 6 H), 0.79 (m, 9 H), 0.93 (m, 9 H), 1.15 (s, 3 H), 1.26 (s, 3 H), 1.74 (s, 3 H), 1.91 (m, 1 H), 2.03 (s, 3 H), 2.19 (s, 3 H), 2.57 (m, 1 H), 2.58 (s, 3 H), 3.43 (dd, *J* = 16.0, 5.5 Hz, 1 H), 3.53 (dd, *J* = 16.0, 5.5 Hz, 1 H), 3.66 (s, 1 H), 3.82 (d, *J* = 7.5 Hz, 1 H), 3.84 (d, *J* = 8.0 Hz, 2 H), 3.91 (dd, *J* = 10.5, 6.5 Hz, 1 H), 4.28 (d, *J* = 9.0 Hz, 1 H), 4.32 (dd, *J* = 10.5, 4.0 Hz, 1 H), 4.47 (m, 3 H), 4.62 (d, *J* = 10.5 Hz, 1 H), 4.71 (d, *J* = 1.5Hz, 1 H), 4.90 (dd, *J* = 17.0, 2.0 Hz, 1 H), 4.99 (m, 2 H), 5.44 (m, 1 H), 5.57 (d, *J* = 8.4 Hz, 1 H), 5.99 (m, 2 H), 6.20 (d, *J* = 7.0 Hz, 1 H), 6.47 (s, 1 H), 6.99 (d, *J* = 8.5 Hz, 1 H), 7.24 (m, 2 H), 7.40 (m, 8 H), 7.57 (t, *J* = 8.0 Hz, 1 H), 8.10 (d, *J* = 7.5 Hz, 2 H); ^{13}C NMR (100.5 MHz, $CDCl_3$) δ 4.6, 5.5, 6.7, 6.9, 10.1, 14.6, 21.1, 23.6, 26.3, 37.5, 43.7, 46.1, 56.2, 59.0, 72.5, 72.8, 75.0, 75.2, 76.7, 76.8, 78.8, 78.9, 81.9, 84.4, 113.8, 116.3, 118.1, 126.6, 126.7, 127.9, 128.2, 128.9, 129.2, 129.8, 130.2, 130.6, 130.8, 133.0, 133.7, 134.5, 135.6, 135.9, 136.5, 137.8, 138.6, 138.8, 138.9, 165.8, 169.1, 169.6, 169.9, 171.7, 201.2. HRMS calculated for $C_{65}H_{87}NO_{15}Si_2H^+$: 1178.5693, found 1178.5703.

Macrocyclic Taxoid SB-T-2053

To a solution of **8** (47 mg, 0.041 mmol) in 23 ml CH_2Cl_2 was added bis(tricyclohexylphosphine)benzylideneruthenium(IV) dichloride ("Grubbs's catalyst," 8 mg, 0.01 mmol) in 0.2 ml CH_2Cl_2. The reaction was stirred overnight. Solvent was removed under reduced pressure. The residue was passed through a short column (eluent Hex/EtOAc, 5/1) to remove remaining catalyst and afford **9** as a crude yellow solid (39 mg, 85%).

To a solution of **9** (50 mg) in CH_3CN (1.0 ml) and pyridine (1.0 ml) was added HF-pyridine (70:30, 0.5 ml), and the reaction mixture was stirred overnight. The reaction mixture was diluted with EtOAc (120 ml) and washed with a saturated aqueous $NaHCO_3$ solution (10 ml × 2), a $CuSO_4$ solution (10 ml × 3), water (10 ml × 3), and brine (3 ml). The organic layer was dried over anhydrous $MgSO_4$, and solvent was removed under reduced pressure. The residue was purified by chromatography using 1/1 Hexanes:EtOAc as the eluent to afford **SB-T-2053** as white solid (37 mg, 93%). Mp: 208°C–210°C. $[\alpha]_D^{22}$ –49 (c 0.92, $CHCl_3$). ^{1}H NMR (500 MHz, $CDCl_3$) δ 1.19 (s, 3 H), 1.23 (s, 3 H), 1.71 (s, 3 H), 1.86 (s, 3 H), 1.91 (m, 1 H), 2.23 (s, 3 H), 2.37 (s, 1 H), 2.55 (s, 3 H), 2.59 (m, 1 H), 2.98 (s, 1 H), 3.23 (d, *J* = 16.0 Hz, 1 H), 3.35 (s, 1 H), 3.81 (d, *J* = 6.6 Hz, 1 H), 3.84 (m, 2 H), 3.88 (d, *J* =8.4 Hz, 1 H), 3.96 (m, 1 H), 4.11 (m, 1 H), 4.25 (d, *J* = 9.0 Hz, 1 H), 4.40 (m, 1 H), 4.45 (d, *J* = 8.4 Hz, 1 H), 4.67 (d, *J* = 1.8 Hz, 1 H), 5.00 (d, *J* =1.2 Hz, 1 H), 5.22 (d, *J* = 5.4 Hz, 1 H), 5.35 (d, *J* = 16.2 Hz, 1 H), 5.56 (m, 1 H), 6.24 (d, *J* = 7.8 Hz, 1 H), 6.29 (s, 1 H), 6.71 (d, *J* = 6.0 Hz, 1 H), 7.17 (d, *J* = 7.2 Hz, 1 H), 7.28-7.53 (m, 9 H), 7.62 (t, *J* = 7.2 Hz, 1 H), 8.09 (d, *J* = 7.2 Hz, 2 H); ^{13}C NMR (100.5 MHz, $CDCl_3$) δ 9.4, 14.8, 20.8, 23.1, 26.2, 35.7, 37.7, 43.5, 44.9, 55.2, 58.9, 72.0, 72.5, 73.2, 74.6, 75.1, 76.2, 79.3, 79.8, 81.7, 84.3, 125.9, 126.5, 126.9, 127.3, 127.6, 128.2, 128.7, 128.9, 129.3, 129.8, 130.5, 131.4, 133.8, 135.0, 135.5, 137.5, 137.7, 138.1, 165.3, 169.2, 169.6, 171.1, 172.9, 203.0. HRMS calculated for $C_{51}H_{56}NO_{15}H^+$: 922.3650, found 922.3659.

Supplemental Data

Two supplemental figures are available online at http://www.chembiol.com/cgi/content/full/12/3/339/DC1/.

Acknowledgments

This work was supported by grants from the National Institutes of Health (GM42798 and CA103314 to I.O., GM6167803 to C.L.S., CA73872 to R.J.B., and CA39821 and CA77263 to S.B.H.) and the National Foundation for Cancer Research (to S.B.H.). I.O. is grateful to Indena, SpA for the generous gift of 14β-hydroxy-10-deacetylbaccatin III.

Received: August 10, 2004
Revised: December 25, 2004
Accepted: January 4, 2005
Published: March 25, 2005

References

1. Wani, M.C., Taylor, H.L., Wall, M.E., Coggon, P., and McPhail, A.T. (1971). Plant antitumor agents.6. Isolation and structure of taxol, a novel antileukemic and antitumor agent from taxus-brevifolia. J. Am. Chem. Soc. *93*, 2325–2327.
2. Gueritte-Voegelein, F., Guenard, D., Mangatal, L., Potier, P., Guilhem, J., Cesario, M., and Pascard, C. (1990). Structure of a synthetic taxol precursor—N-tert-butoxycarbonyl-10-deacetyl-n-debenzoyltaxol. Acta Crystallogr. C *46*, 781–784.
3. Crown, J., O'Leary, M., and Ooi, W.S. (2004). Docetaxel and paclitaxel in the treatment of breast cancer: A review of clinical experience. Oncologist *9*, 24–32.
4. Crown, J., and O'Leary, M. (2000). The taxanes: An update. Lancet *355*, 1176–1178.
5. Rowinsky, E.K. (1997). The development and clinical utility of the taxane class of antimicrotubule chemotherapy agents. Annu. Rev. Med. *48*, 353–374.
6. Schiff, P.B., Fant, J., and Horwitz, S.B. (1979). Promotion of microtubule assembly in vitro by taxol. Nature *277*, 665–667.
7. Schiff, P.B., and Horwitz, S.B. (1980). Taxol stabilizes microtubules in mouse fibroblast cells. Proc. Natl. Acad. Sci. USA *77*, 1561–1565.
8. Horwitz, S.B. (1992). Mechanism of action of taxol. Trends Pharmacol. Sci. *13*, 134–136.
9. Yvon, A.M.C., Wadsworth, P., and Jordan, M.A. (1999). Taxol suppresses dynamics of individual microtubules in living human tumor cells. Mol. Biol. Cell *10*, 947–959.
10. Lin, S., and Ojima, I. (2000). Recent strategies in the development of taxane anticancer drugs. Expert Opin. Ther. Patents *10*, 869–889.
11. Gueritte, F. (2001). General and recent aspects of the chemistry and structure-activity relationships of taxoids. Curr. Pharm. Des. *7*, 1229–1249.
12. Dubois, J., Guenard, D., and Gueritte, F. (2003). Recent developments in antitumour taxoids. Expert Opin. Ther. Patents *13*, 1809–1823.
13. Nogales, E., Wolf, S.G., and Downing, K.H. (1998). Structure of the alpha beta tubulin dimer by electron crystallography. Nature *391*, 199–203.
14. Loewe, J., Li, H., Downing, K.H., and Nogales, E. (2001). Refined structure of alpha beta-tubulin at 3.5 A resolution. J. Mol. Biol. *313*, 1045–1057.
15. Ojima, I., Kuduk, S.D., Chakravarty, S., Ourevitch, M., and Begue, J.P. (1997). A novel approach to the study of solution structures and dynamic behavior of paclitaxel and docetaxel using fluorine-containing analogs as probes. J. Am. Chem. Soc. *119*, 5519–5527.
16. Ojima, I., Inoue, T., and Chakravarty, S. (1999). Enantiopure fluorine-containing taxoids: Potent anticancer agents and versatile probes for biomedical problems. J. Fluor. Chem. *97*, 3–10.
17. Li, Y.K., Poliks, B., Cegelski, L., Poliks, M., Gryczynski, Z., Piszczek, G., Jagtap, P.G., Studelska, D.R., Kingston, D.G.I., Schaefer, J., et al. (2000). Conformation of microtubule-bound paclitaxel determined by fluorescence spectroscopy and REDOR NMR. Biochemistry *39*, 281–291.
18. Rao, S., Krauss, N.E., Heerding, J.M., Swindell, C.S., Ringel, I., Orr, G.A., and Horwitz, S.B. (1994). 3′-(p-azidobenzamido)taxol photolabels the N-terminal 31 amino-acids of beta-tubulin. J. Biol. Chem. *269*, 3132–3134.
19. Rao, S., Orr, G.A., Chaudhary, A.G., Kingston, D.G.I., and Horwitz, S.B. (1995). Characterization of the taxol binding-site on the microtubule-2-(m-azidobenzoyl)taxol photolabels a pep-

tide (amino-acids 217- 231) of beta-tubulin. J. Biol. Chem. *270*, 20235–20238.
20. Rao, S., He, L., Chakravarty, S., Ojima, I., Orr, G.A., and Horwitz, S.B. (1999). Characterization of the taxol binding site on the microtubule. Identification of Arg(282) in beta-tubulin as the site of photoincorporation of a 7-benzophenone analogue of taxol. J. Biol. Chem. *274*, 37990–37994.
21. Ojima, I., Chakravarty, S., Inoue, T., Lin, S.N., He, L.F., Horwitz, S.B., Kuduk, S.D., and Danishefsky, S.J. (1999). A common pharmacophore for cytotoxic natural products that stabilize microtubules. Proc. Natl. Acad. Sci. USA *96*, 4256–4261.
22. Snyder, J.P., Nettles, J., Cornett, B., Downing, K.H., and Nogales, E. (2001). The binding conformation of taxol in beta-tubulin: A model based on electron crystallographic density. Proc. Natl. Acad. Sci. USA *98*, 5312–5316.
23. Giannakakou, P., Gussio, R., Nogales, E., Downing, K.H., Zaharevitz, D., Bollbuck, B., Poy, G., Sackett, D., Nicolaou, K.C., and Fojo, T. (2000). A common pharmacophore for epothilone and taxanes: Molecular basis for drug resistance conferred by tubulin mutations in human cancer cells. Proc. Natl. Acad. Sci. USA *97*, 2904–2909.
24. Barboni, L., Lambertucci, C., Appendino, G., Vander Velde, D.G., Himes, R.H., Bombardelli, E., Wang, M.M., and Snyder, J.P. (2001). Synthesis and NMR-driven conformational analysis of taxol analogues conformationally constrained on the C13 side chain. J. Med. Chem. *44*, 1576–1587.
25. Ojima, I., Lin, S., Inoue, T., Miller, M.L., Borella, C.P., Geng, X., and Walsh, J.J. (2000). Macrocycle formation by ring-closing metathesis. Application to the syntheses of novel macrocyclic taxoids. J. Am. Chem. Soc. *122*, 5343–5353.
26. Boge, T.C., Wu, Z.J., Himes, R.H., Vander Velde, D.G., and Georg, G.I. (1999). Conformationally restricted paclitaxel analogues: Macrocyclic mimics of the "hydrophobic collapse" conformation. Bioorg. Med. Chem. Lett. *9*, 3047–3052.
27. Ojima, I., Geng, X., Lin, S., Pera, P., and Bernacki, R.J. (2002). Design, synthesis and biological activity of novel C2–C3′ N-linked macrocyclic taxoids. Bioorg. Med. Chem. Lett. *12*, 349–352.
28. Metaferia, B.B., Hoch, J., Glass, T.E., Bane, S.L., Chatterjee, S.K., Snyder, J.P., Lakdawala, A., Cornett, B., and Kingston, D.G.I. (2001). Synthesis and biological evaluation of novel macrocyclic paclitaxel analogues. Org. Lett. *3*, 2461–2464.
29. Ganesh, T., Guza, R.C., Bane, S., Ravindra, S., Shanker, N., Lakdawala, A.S., Snyder, J.P., and Kingston, D.G.I. (2004). The bioactive taxol conformation on beta-tubulin: Experimental evidence from highly active constrained analogs. Proc. Natl. Acad. Sci. USA *101*, 10006–10011.
30. Wilson, L., and Jordan, M.A. (1995). Microtubule dynamics: taking aim at a moving target. Chem. Biol. *2*, 569–573.
31. Williams, H.J., Scott, A.I., Dieden, R.A., Swindell, C.S., Chirlian, L.E., Francl, M.M., Heerding, J.M., and Krauss, N.E. (1993). NMR and molecular modeling study of the conformations of taxol and of its side-chain methylester in aqueous and nonaqueous solution. Tetrahedron *49*, 6545–6560.
32. Dubois, J., Guenard, D., Gueritte-Voegelein, F., Guedira, N., Potier, P., Gillet, B., and Beloeil, J.C. (1993). Conformation of taxotere and analogs determined by NMR-spectroscopy and molecular modeling studies. Tetrahedron *49*, 6533–6544.
33. Vandervelde, D.G., Georg, G.I., Grunewald, G.L., Gunn, G.W., and Mitscher, L.A. (1993). Hydrophobic collapse of taxol and taxotere solution conformations in mixtures of water and organic solvent. J. Am. Chem. Soc. *115*, 11650–11651.
34. Mastropaolo, D., Camerman, A., Luo, Y.G., Brayer, G.D., and Camerman, N. (1995). Crystal and molecular structure of paclitaxel (taxol). Proc. Natl. Acad. Sci. USA *92*, 6920–6924.
35. Nicklaus, M.C., Wang, S.M., Driscoll, J.S., and Milne, G.W.A. (1995). Conformational changes of small molecules binding to proteins. Bioorg. Med. Chem. *3*, 411–428.
36. Chang, G., Guida, W.C., and Still, W.C. (1989). An internal coordinate Monte-Carlo method for searching conformational space. J. Am. Chem. Soc. *111*, 4379–4386.
37. Dorman, G., and Prestwich, G.D. (1994). Benzophenone photophores in biochemistry. Biochemistry *33*, 5661–5673.
38. Geng, X., Miller, M.L., Lin, S., and Ojima, I. (2003). Synthesis of novel C2–C3′ N-linked macrocyclic taxoids by means of highly regioselective Heck macrocyclization. Org. Lett. *5*, 3733–3736.
39. Grubbs, R.H., and Chang, S. (1998). Recent advances in olefin metathesis and its application in organic synthesis. Tetrahedron *54*, 4413–4450.
40. Ojima, I. (1995). Recent advances in the beta-lactam synthon method. Acc. Chem. Res. *28*, 383–389.
41. Ojima, I., Kuduk, S.D., and Chakravarty, S. (1998). Recent advances in the medicinal chemistry of taxoid anticancer agents. In Advances in Medicinal Chemistry, Volume 4, B.E. Maryanoff and A.B. Reitz, eds. (Greenwich, CT: JAI Press), pp. 69–124.
42. Ojima, I., Habus, I., Zhao, M., Zucco, M., Park, Y.H., Sun, C.M., and Brigaud, T. (1992). New and efficient approaches to the semisynthesis of taxol and its C-13 side-chain analogs by means of beta-lactam synthon method. Tetrahedron *48*, 6985–7012.
43. Ojima, I., Slater, J.C., Kuduk, S.D., Takeuchi, C.S., Gimi, R.H., Sun, C.M., Park, Y.H., Pera, P., Veith, J.M., and Bernacki, R.J. (1997). Syntheses and structure-activity relationships of taxoids derived from 14-beta-hydroxy-10-deacetylbaccatin III. J. Med. Chem. *40*, 267–278.
44. Crich, D., and Yao, Q. (1996). Generation of acyl radicals from thiolesters by intramolecular homolytic substitution at sulfur. J. Org. Chem. *61*, 3566–3570.
45. Appendino, G., Gariboldi, P., Gabetta, B., Pace, R., Bombardelli, E., and Viterbo, D. (1992). 14-beta-hydroxy-10-deacetylbaccatin-III, a new taxane from himalayan yew (taxus-wallichiana zucc). J. Chem. Soc. [Perkin 1] *1*, 2925–2929.
46. Ford, J.M., and Hait, W.N. (1990). Pharmacology of drugs that alter multidrug resistance in cancer. Pharmacol. Rev. *42*, 155–199.
47. Gottesman, M.M., and Pastan, I. (1993). Biochemistry of multidrug resistance mediated by the multidrug transporter. Annu. Rev. Biochem. *62*, 385–427.
48. Still, W.C., Tempczyk, A., Hawley, R.C., and Hendrickson, T. (1990). Semianalytical treatment of solvation for molecular mechanics and dynamics. J. Am. Chem. Soc. *112*, 6127–6129.
49. Weisenberg, R.C. (1972). Microtubule formation in-vitro in solutions containing low calcium concentrations. Science *177*, 1104–1105.
50. Shelanski, M.L., Gaskin, F., and Cantor, C.R. (1973). Microtubule assembly in absence of added nucleotides. Proc. Natl. Acad. Sci. USA *70*, 765–768.
51. Skehan, P., Storeng, R., Scudiero, D., Monks, A., McMahon, J., Vistica, D., Warren, J., Bokesch, H., Kenney, S., and Boyd, M. (1990). New colorimetric cytotoxicity assay for anticancer-drug screening. J. Natl. Cancer Inst. *82*, 1107–1112.
52. Motulsky, H.J., and Ransnas, L.A. (1987). Fitting curves to data using nonlinear regression - a practical and nonmathematical review. FASEB J. *1*, 365–374.
53. Geney, R., Geng, X.D., Simmerling, C., and Ojima, I. (2002). Rational design and evaluation of conformationally restrained taxoids. Abstr. Pap. Am. Chem. Soc. *224*, MEDI-139.